Stanford Exploration Project, Report 129, May 6, 2007, pages 65–75

Target-oriented wave-equation inversion: Sigsbee model

Alejandro A. Valenciano

ABSTRACT

A complex velocity model can cause shadow zones in an image computed by migration due to poor illumination. These shadow zones may contain weak signals masked by artifacts. To reduce artifacts and recover the real signal, a target-oriented wave-equation inversion scheme can be developed that uses an explicitly computed least squares inversion Hessian. To solve the otherwise ill-conditioned inversion problem a model regularization needs to be added. One choice for regularization is to use the customary damping in the image space, another is to penalize the energy in the image not focused at zero subsurface-offset. To apply the second, the subsurface-offset Hessian needs to be computed by using the adjoint of migration as the modeling operator. Results on Sigsbee model show encouraging results.

INTRODUCTION

Conventional imaging techniques such as migration cannot provide an accurate picture of poorly illuminated areas (Clapp, 2005). In such areas, migration artifacts can easily obscure the small amount of signal that exists. One way to solve this problem is to use an inversion formalism introduced by Tarantola (1987) to solve geophysical imaging problems. This procedure computes an image by weighting the migration result with the inverse of the Hessian matrix.

However, when the dimensions of the problem get large, the explicit calculation of the Hessian matrix and its inverse becomes unfeasible. That is why the following approximation to the wave-equation inversion must be performed: (1) to compute the Hessian in a target-oriented fashion to reduce the size of the problem; (2) to exploit the sparse structure of the Hessian matrix; and (3) to compute the inverse image following a iterative inversion scheme. The last item renders unnecessary an explicit computation of inverse of the Hessian matrix.

In this paper, I apply the target-oriented wave-equation inversion to the Sigsbee data set. I show postack (zero subsurface-offset) and prestack (subsurface-offset) image space inversion results. I use a customary damping model regularization to make the postack inversion stable. By the other hand, the prestack inversion is stabilized by using a regularization that penalizes energy not focused at zero subsurface-offset (Shen et al., 2003).

LINEAR LEAST-SQUARES INVERSION

Tarantola (1987) formalizes the geophysical inverse problem by giving a theoretical approach to compensate for experimental deficiency (e.g., acquisition geometry, complex overburden), while being consistent with the acquired data. His approach can be summarized as follows: given a linear modeling operator $\mathbf{L}$, compute synthetic data $\mathbf{d}$ using $\mathbf{d} = \mathbf{L}\mathbf{m}$ where $\mathbf{m}$ is a reflectivity model. Given the recorded data $\mathbf{d}_{obs}$, a quadratic cost function,

$$S(\mathbf{m}) = \|\mathbf{d} - \mathbf{d}_{obs}\|^2 = \|\mathbf{L}\mathbf{m} - \mathbf{d}_{obs}\|^2, \tag{1}$$

is formed. The reflectivity model $\hat{\mathbf{m}}$ that minimizes $S(\mathbf{m})$ is given by the following:

$$\hat{\mathbf{m}} = (\mathbf{L}'\mathbf{L})^{-1}\mathbf{L}'\mathbf{d}_{obs} = \mathbf{H}^{-1}\mathbf{m}_{mig}, \tag{2}$$

where $\mathbf{L}'$ (migration operator) is the adjoint of the linear modeling operator $\mathbf{L}$, $\mathbf{m}_{mig}$ is the migration image, and $\mathbf{H} = \mathbf{L}'\mathbf{L}$ is the Hessian of $S(\mathbf{m})$.

The main difficulty with this approach is the explicit calculation of the Hessian inverse. In practice, it is more feasible to compute the least-squares inverse image as the solution of the linear system of equations,

$$\mathbf{H}\hat{\mathbf{m}} = \mathbf{m}_{mig}, \tag{3}$$

by using an iterative inversion algorithm.

Regularization in the postack image space

The condition number of the target-oriented Hessian matrix can be high, making the solution of the non-stationary least-squares filtering problem in equation (3) unstable. One solution is adding a smoothing regularization operator to equation (3):

$$\begin{aligned} \mathbf{H}\hat{\mathbf{m}} - \mathbf{m}_{mig} &\approx 0, \\ \epsilon\mathbf{I}\hat{\mathbf{m}} &\approx 0, \end{aligned} \tag{4}$$

where the choice of the identity operator ($\mathbf{I}$) as regularization operator is customary. A more sophisticated regularization scheme could involve applying a smoothing operator in the reflection angle (or offset ray-parameter) dimension (Prucha et al., 2000; Kuehl and Sacchi, 2001) or, more generally, in the reflection and azimuth angles.

Regularization in the prestack image space

The previous subsection solve equation 3 in a poststack image domain (zero subsurface-offset). But a prestack regularization is necessary to reduce the noise in the inversion result. If subsurface offset is included in the computation of the Hessian, a generalization to the prestack image domain of equation 4 is possible.

Three different regularization schemes for wave-equation inversion have been discussed in the literature. First, an identity operator which is customary in many scientific applications (damping). Second, a geophysical regularization which penalizes the roughness of the image in the offset ray parameter dimension (which is equivalent the reflection angle dimension) (Prucha et al., 2000; Kuehl and Sacchi, 2001). Third, a differential semblance operator to penalize the energy in the image not focused at zero subsurface-offset (Shen et al., 2003). In this paper I use the third regularization scheme, the regularization in the reflection angle domain.

A generalization to the prestack image domain of equation 3 needs regularization to obtain a stable solution. The first option for regularization is a customary damping that can be stated as follows:

$$\begin{aligned} \mathbf{H}(\mathbf{x},\mathbf{h};\mathbf{x}',\mathbf{h}')\hat{\mathbf{m}}(\mathbf{x},\mathbf{h}) - \mathbf{m}_{mig}(\mathbf{x},\mathbf{h}) &\approx 0, \\ \varepsilon \mathbf{I}\hat{\mathbf{m}}(\mathbf{x},\mathbf{h}) &\approx 0, \end{aligned} \tag{5}$$

where $\mathbf{x} = (z,x,y)$ is a point in the image, and $\mathbf{h} = (h_x,h_y,h_z)$ is the half subsurface-offset. The subsurface-offset Hessian $\mathbf{H}(\mathbf{x},\mathbf{h};\mathbf{x}',\mathbf{h}')$ is

$$\mathbf{H}(\mathbf{x},\mathbf{h};\mathbf{x}',\mathbf{h}') = \sum_{\omega} \sum_{\mathbf{x}_s} \mathbf{G}'(\mathbf{x}-\mathbf{h},\mathbf{x}_s;\omega)\mathbf{G}(\mathbf{x}'+\mathbf{h}',\mathbf{x}_s;\omega) \sum_{\mathbf{x}_r} \mathbf{G}'(\mathbf{x}+\mathbf{h},\mathbf{x}_r;\omega)\mathbf{G}(\mathbf{x}'-\mathbf{h}',\mathbf{x}_r;\omega),$$

where $\mathbf{G}(\mathbf{x},\mathbf{x}_s;\omega)$ and $\mathbf{G}(\mathbf{x},\mathbf{x}_r;\omega)$ are the Green functions from shot position $\mathbf{x}_s$ and receiver position $\mathbf{x}_r$ to a model space point $\mathbf{x}$.

The third regularization option for the prestack generalization of equation 3, is penalizing the energy in the image not focused at zero subsurface-offset. This is obtained using the fitting goals,

$$\begin{aligned} \mathbf{H}(\mathbf{x},\mathbf{h};\mathbf{x}',\mathbf{h}')\hat{\mathbf{m}}(\mathbf{x},\mathbf{h}) - \mathbf{m}_{mig}(\mathbf{x},\mathbf{h}) &\approx 0, \\ \varepsilon \mathbf{P}_{\mathbf{h}}\hat{\mathbf{m}}(\mathbf{x},\mathbf{h}) &\approx 0, \end{aligned} \tag{6}$$

where $\mathbf{P}_{\mathbf{h}} = |\mathbf{h}|$ is the differential semblance operator (Shen et al., 2003). The only difference between equations 5 and 6 is in the regularization operator.

In the next section I compare the numerical solution of the inversion problems stated in equations 5 and 6 to the imaging of Sigsbee model.

NUMERICAL RESULTS: SIGSBEE MODEL

The Sigsbee data set was modeled by simulating the geological setting found on the Sigsbee escarpment in the deep-water Gulf of Mexico. The model exhibits the illumination problems due to the complex salt shape, characterized by a rugose salt top (see Figure 1). We choose a target zone (see Figure 4) to see the effects of illumination on imaging close to the salt.

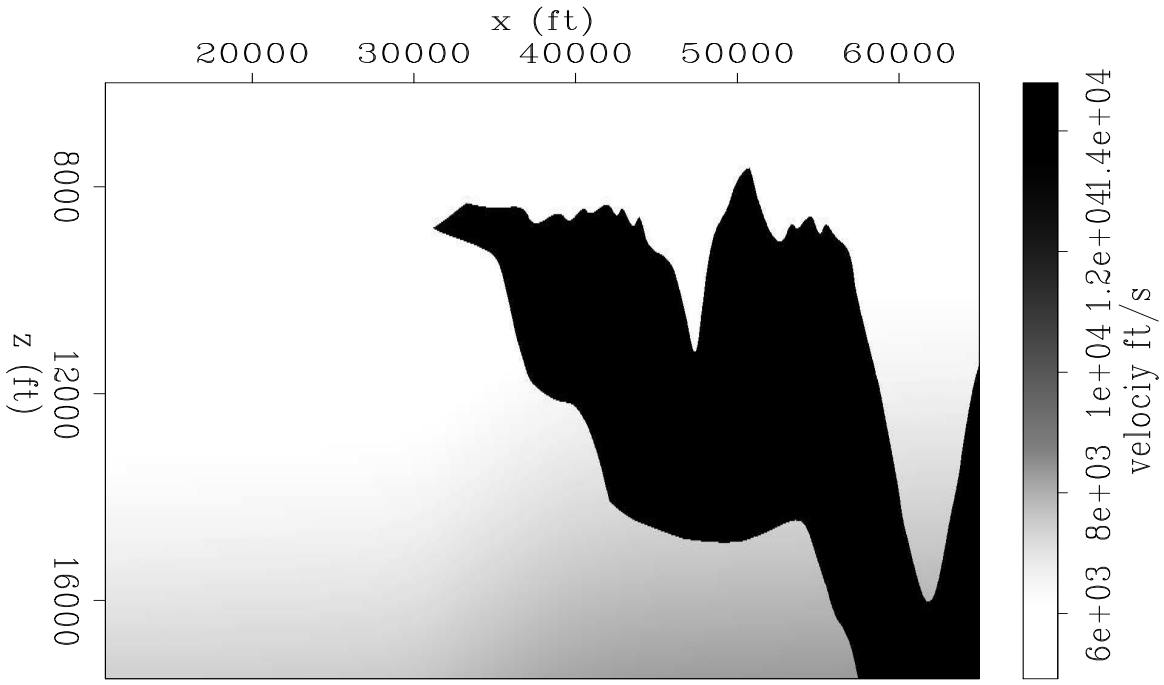

Figure 1: Sigsbee velocity model. alejandro2-Sis_vel [ER]

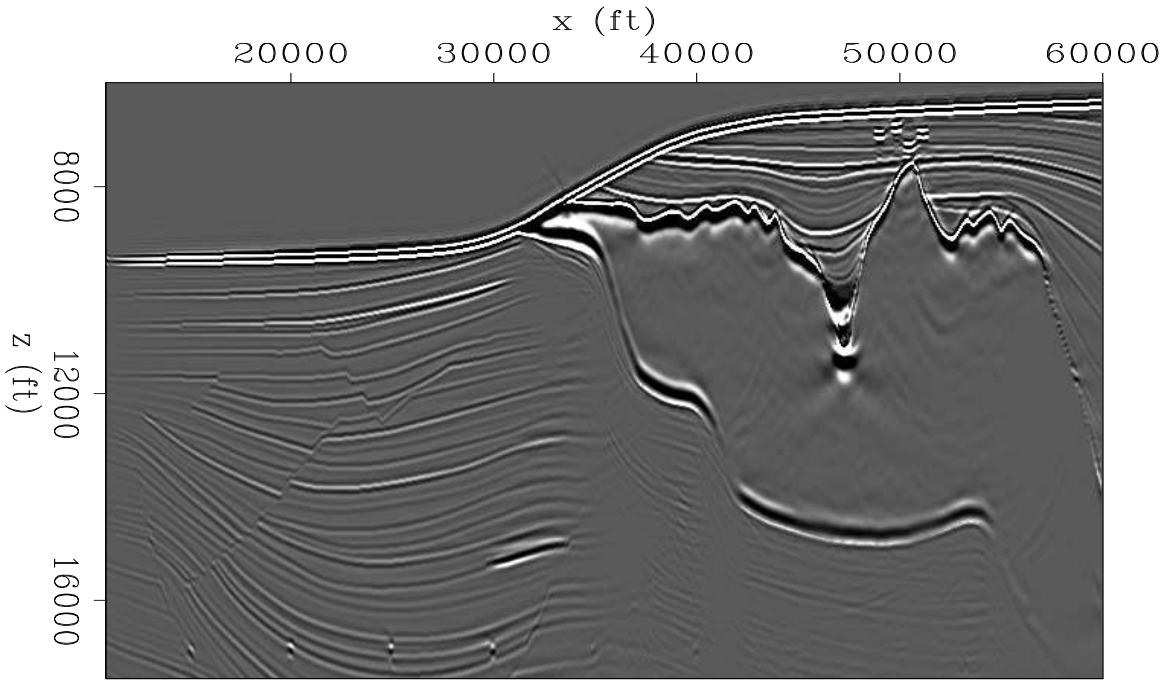

Figure 2: Sigsbee shot-profile migration image using cross-correlation imaging condition. alejandro2-mig_Sis [CR]

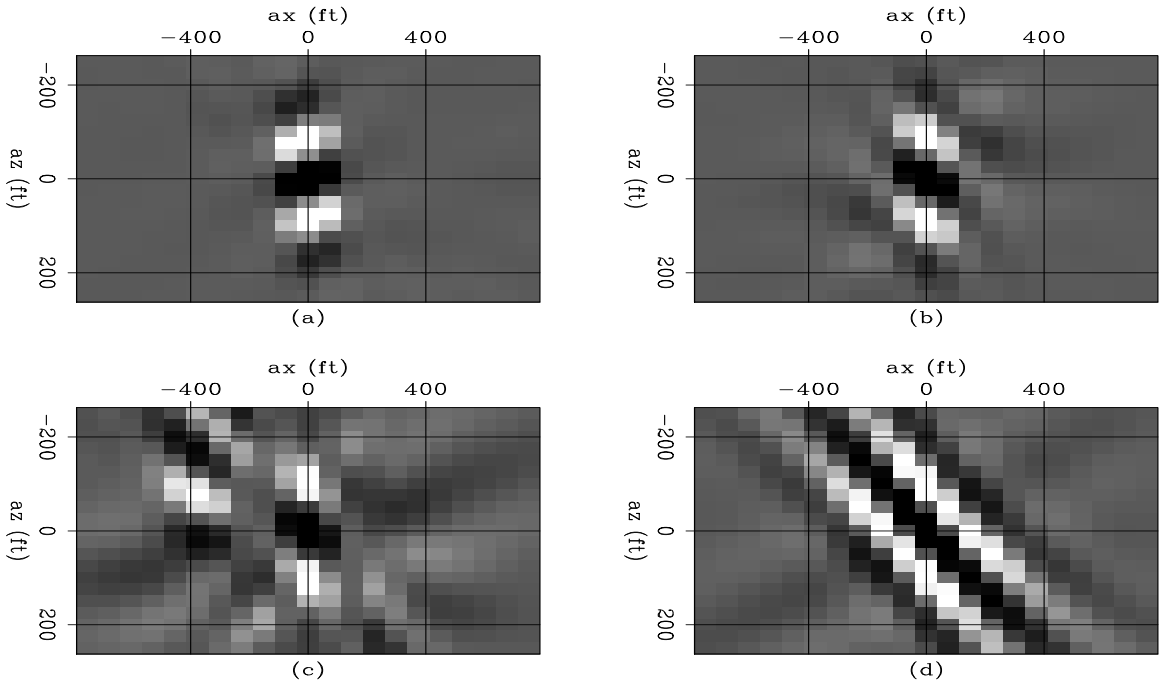

Figure 3: Hessian of the Sigsbee model, (a) point 1 $\mathbf{x} = (12000, 32000)\, ft$, (b) point 2 $\mathbf{x} = (12000, 33500)\, ft$, (c) point 3 $\mathbf{x} = (12000, 35000)\, ft$, and (d) point 4 $\mathbf{x} = (12000, 36500)\, ft$. alejandro2-hesian_phase_Sis [CR]

Figure 2 shows the shot-profile migration image (using cross-correlation imaging condition) corresponding to the portion of Sigsbee model shown in figure 1. Notice how the amplitudes of the reflectors fade away as they get closer to the salt.

Figure 3 shows a 21×21 coefficient filter (target-oriented Hessian) at constant depth as the x coordinate moves from the sediments to the salt boundary. Figure 3a shows point 1, with coordinates $\mathbf{x} = (12000, 32000)\, ft$ (far from the salt). Figure 3b shows point 2, with coordinates $\mathbf{x} = (12000, 33500)\, ft$. Figure 3c shows point 3, with coordinates $\mathbf{x} = (12000, 35000)\, ft$. Figure 3d shows point 4, with coordinates $\mathbf{x} = (12000, 36500)\, ft$.

The shape of the filter is not dependent only on the acquisition geometry but the subsurface geometry (presence of the salt body). In the area unaffected by the salt the filter looks the same as is the constant velocity case, but as we get closer to the salt the illumination varies (in intensity and angle) and the filter behaves differently. This is due to a focusing and defocusing effect created by the salt. To correct this effect we computed the least-squares inverse image.

Figure 5 shows a comparison between the migration and the postack inversion images in the target area. The reflection coefficients are shown in Figure 4a. Notice the position of the faults. Figure 4b shows the illumination, which is the diagonal of the Hessian matrix. Notice the decrease in the illumination as it gets closer to the salt with the exception of a narrow strip where energy focuses close to the salt. The migration result is shown in Figure 5a. The reflectors dim out as they get closer to the salt. In contrast, Figure 5b shows the postack

inversion result, the resolution increases and the section looks more balanced. The fault can be followeded and interpreted closer to the salt body.

The salt, in the inversion image looks distorted. This is due to the fact that data values (migration) in the salt boundary are bigger than everywhere else (Figure 5a), and so are the data residuals. Thus, the solver expends most of the time decreasing the residuals in that area. A residual weight designed to decrease the salt contribution should improve the image. Figures 6 and 7 compare the migration and the prestack inversion images in the reduced target area. The resolution increases, and the section looks more balanced in the prestack inversion result. The fault can be follow and interpreted closer to the salt body in the inversion image.

CONCLUSIONS

A generalization of the wave-equation target-oriented inversion to the prestack image domain needs regularization, since the condition number of the target-oriented Hessian matrix can be high. In general, inversion gives more balanced sections and higher resolution images. However, it also increases the noise that is not modeled by the one-way Green functions.

While imaging the Sigsbee model, both postack and prestack inversion methods obtained better zero subsurface-offset images than migration, increasing the resolution and the continuity of the events into the shadow zones.

ACKNOWLEDGMENTS

I would like to thank the SMAART JV for the synthetic data used in the experiments, as well as the Stanford Exploration Project sponsors for financial and technical support.

REFERENCES

Clapp, M. L., 2005, Imaging under salt: illumination compensation by regularized inversion: Ph.D. thesis, Stanford University.

Kuehl, H. and M. Sacchi, 2001, Generalized least-squares DsR migration using a common angle imaging condtion: Generalized least-squares DsR migration using a common angle imaging condtion:, Soc. of Expl. Geophys., 71st Ann. Internat. Mtg, 1025–1028.

Prucha, M. L., R. G. Clapp, and B. Biondi, 2000, Seismic image regularization in the reflection angle domain: SEP–**103**, 109–119.

Shen, P., W. Symes, and C. C. Stolk, 2003, Differential semblance velocity analysis by wave-equation migration: 73st Annual International Meeting, SEG, Expanded Abstracts, 2132–2135.

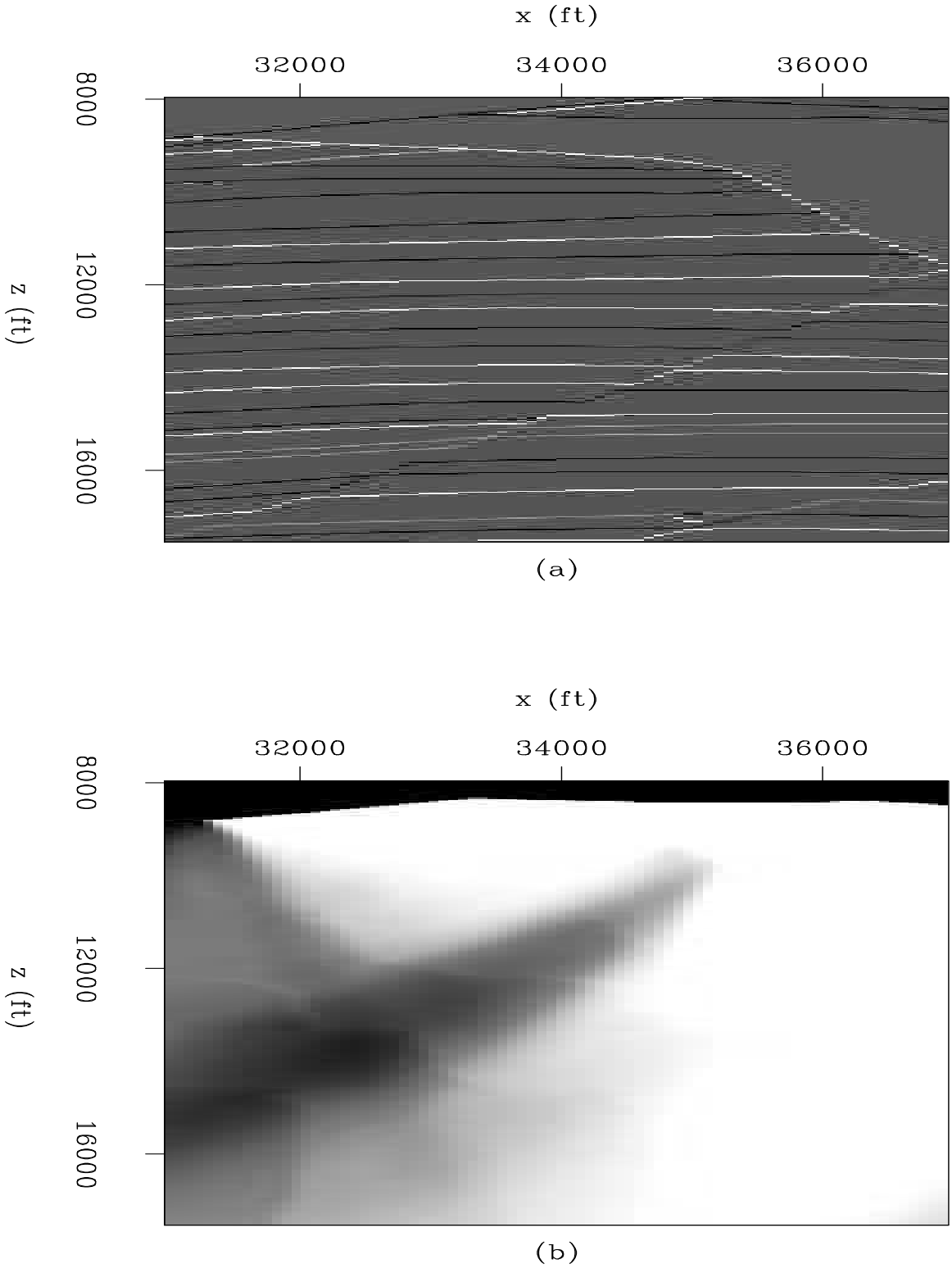

Figure 4: Target area comparison. (a) reflection coefficients, and (b) illumination (dark is high and light is low) alejandro2-comp_Sis_full1 [CR]

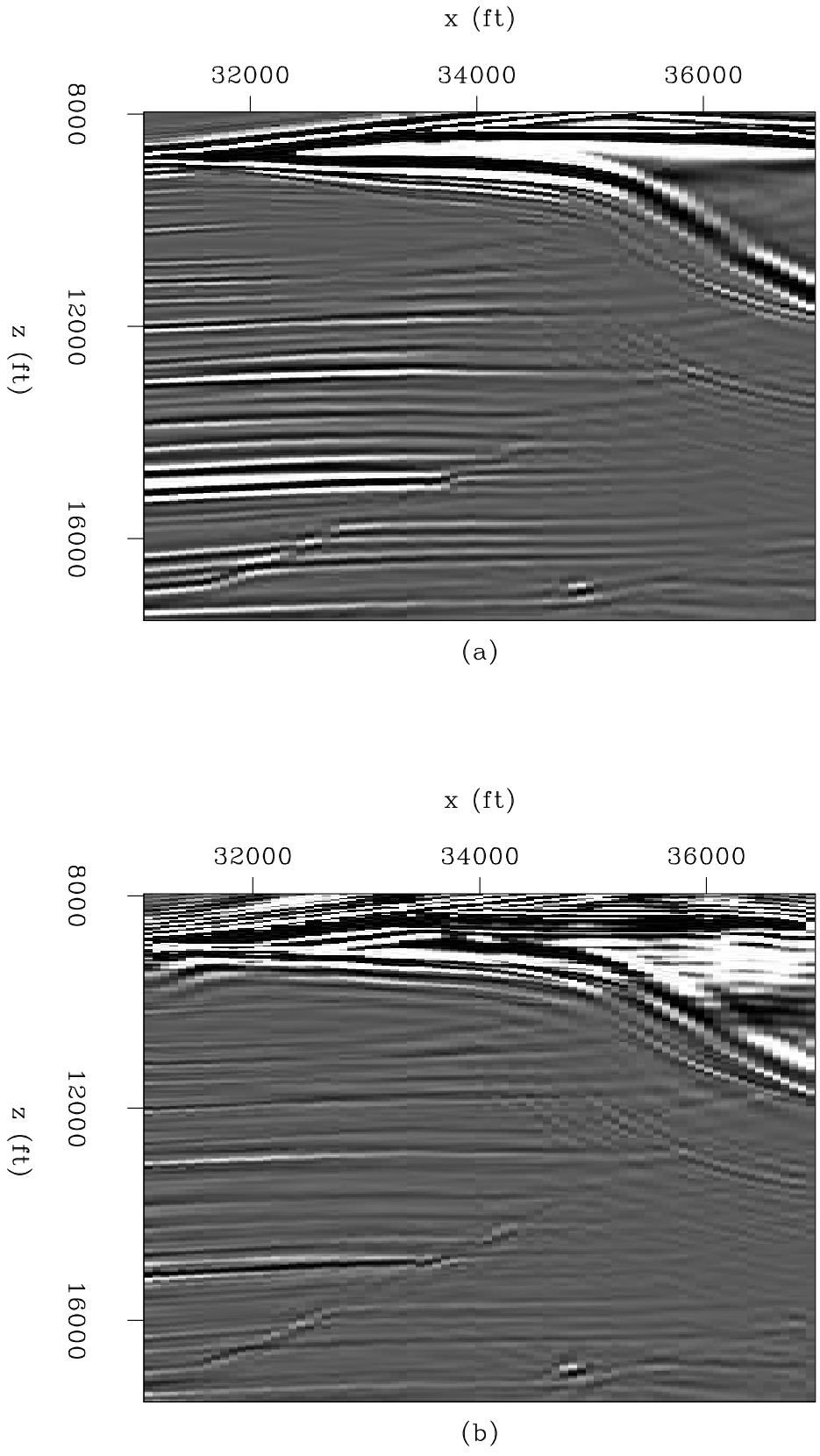

Figure 5: Target area comparison. (a) zero subsurface-offset migration, and (b) inversion. alejandro2-comp_Sis_full2 [CR]

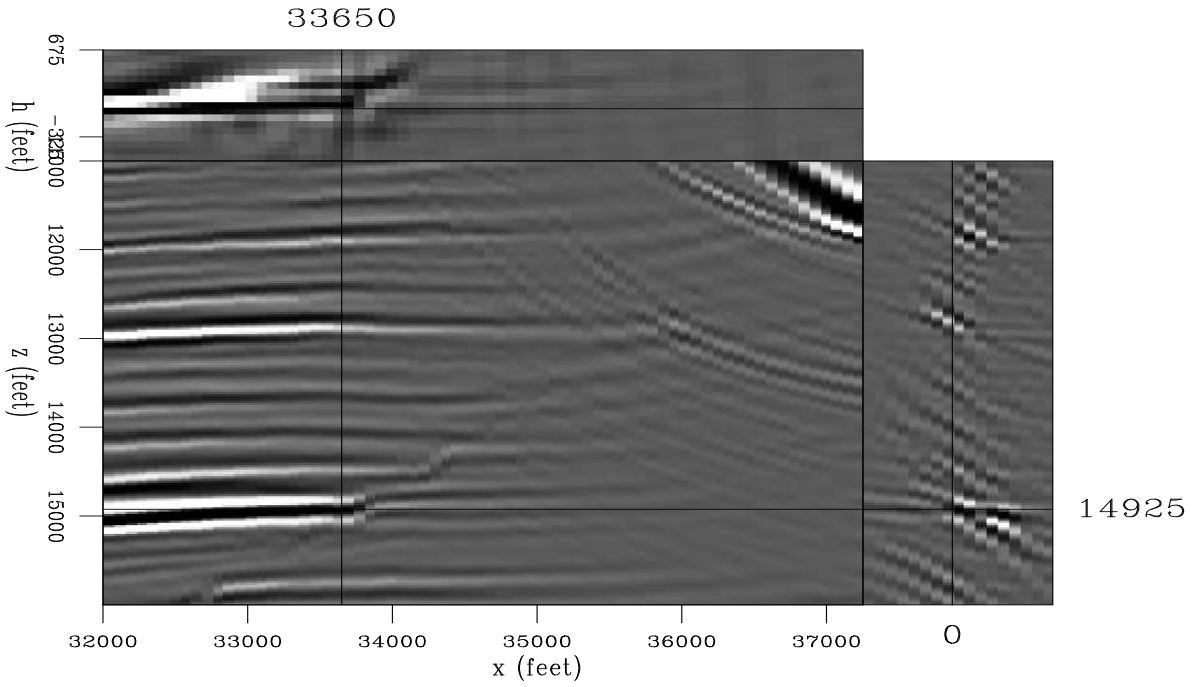

Figure 6: Sigsbee shot-profile migration prestack image using cross-correlation imaging condition. alejandro2-mig_off [CR]

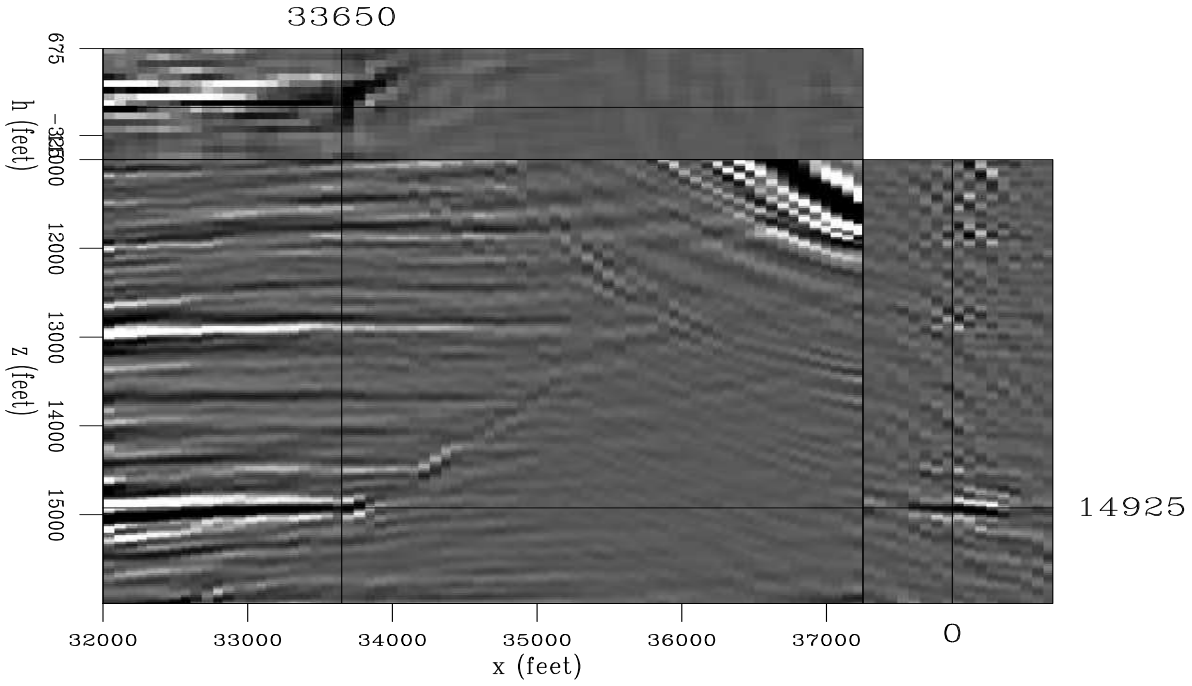

Figure 7: Sigsbee shot-profile inversion prestack image. alejandro2-mig_inv1 [CR]

Tarantola, A., 1987, Inverse problem theory: Methods for data fitting and model parameter estimation: Elsevier Science Publication Company, Inc.